Journal of Photochemistry and Photobiology A: Chemistry 217 (2011) 125–135

Contents lists available at ScienceDirect

Journal of Photochemistry and Photobiology A: Chemistry

journal homepage: www.elsevier.com/locate/jphotochem

Tetrakis(4-sulfonatophenyl)porphyrin fluorescence as reporter of human serum albumin structural changes induced by guanidine hydrochloride

Suzana M. Andrade*, Sílvia M.B. Costa[1]

Centro de Química Estrutural, Complexo 1, Instituto Superior Técnico, Av. Rovisco Pais 1, 1049-001 Lisboa Codex, Portugal

ARTICLE INFO

Article history:
Received 9 July 2010
Received in revised form
24 September 2010
Accepted 28 September 2010
Available online 7 October 2010

Keywords:
HSA
Porphyrin
Aggregation
Chemical unfolding
Fluorescence
FCS

ABSTRACT

The interaction of the drug carrier protein human serum albumin (HSA) with the ionic, free base porphyrin tetrakis(4-sulfonatophenyl)porphyrin (TSPP) was investigated under chemical denaturation conditions using guanidine hydrochloride (Gdn-HCl) in aqueous solution at pH 7 and 2.5. Protein stability was studied by fluorescence spectroscopy using intrinsic tryptophan fluorescence, whereas far-UV circular dichroism gave information regarding conformational changes. Steady-state and time-resolved fluorescence as well as extinction and induced visible CD of TSPP were also monitored in the presence of the denaturant.

The addition of 1.0 M Gdn-HCl inhibited the FRET process between the sole tryptophan residue of HSA and the porphyrin as inferred by an increase in the intrinsic fluorescence of the former together with a drop in the fluorescence of the latter. Simultaneously, an induced bisignate CD band was detected in the Soret region of TSPP extinction following the changes in the monomer ↔ aggregate equilibrium of TSPP. The features in the extinction spectra pointed to the formation of J-aggregates at pH = 2.5 and were confirmed by fluorescence lifetime measurements. At pH = 7, no TSPP dimers were detected in the absence of the protein or in the presence of native HSA. However, H-dimers or higher aggregates of TSPP associated to HSA were induced at concentrations of Gdn-HCl below 2 M.

The main unfolding transition probed by HSA intrinsic fluorescence took place between 2 and 3 M Gdn-HCl at pH = 7, whereas at pH = 2.5 it was detected only above 2.8 M Gdn-HCl, coinciding with TSPP release into solution which occurs at high denaturant concentration for both pH studied. The results suggest that the chemical unfolding of HSA is a multistep process. The free base porphyrin contributes to an increase in the protein stability, particularly important under acidic conditions, where the protein is known to be in an expanded form in the absence of TSPP.

The analysis of TSPP fluorescence fluctuations in the autocorrelation functions obtained using fluorescence correlation spectroscopy (FCS) in the presence of HSA at different denaturant concentrations showed that the porphyrin only interacts with the native form of the protein.

Both fluorescence and circular dichroism data confirmed that in the noncovalent complex HSA–TSPP the free base porphyrin can act as a reporter of the protein structural changes induced either by pH or chemical denaturation.

1. Introduction

The ability of proteins to alter their conformational and dynamic properties as a result of association with small molecules can be decisive for their correct function. Despite the recognized importance of this modulation mechanism, it remains a challenge to investigate the ways in which the binding at a specific site is sensed throughout a protein structure, and triggers a response to the association reaction [1]. The albumins' ability to bind and transport a large variety of ligands, including fatty acids, metabolites and drugs, makes them interesting model systems for ligand-binding studies [2]. In some pathogenic states of albumins, weaker interactions lead to an increase of drug concentration in the blood serum which in turn can cause toxic poisoning or even death. Likewise, ligand binding can induce structural modifications in the protein with positive implications: certain metal derivatives of *meso*-tetra(4-sulfonatophenyl)porphine (TSPP) were effective at inhibiting insulin aggregation [3]. Hence, studies involving the interaction of drugs (ligands) with the native and unfolded states of proteins remain pertinent.

The importance of porphyrins and related compounds as therapeutic drugs and targeting agents has been widely recognized. Its high affinity to tumors makes them promising compounds for photodynamic therapy [4] as well as potential MRI contrast agents [5]. Thus, a better understanding of the interaction of water-soluble porphyrins with cellular targets like membranes, proteins or nucleic acids is essential [6].

* Corresponding author. Tel.: +351 21 8419389; fax: +351 21 8464455.
E-mail address: suzana.andrade@ist.utl.pt (S.M. Andrade).
[1] Fax: +351 21 8464455.

1010-6030/$ – see front matter © 2010 Elsevier B.V. All rights reserved.
doi:10.1016/j.jphotochem.2010.09.028

Alterations of physicochemical properties of porphyrins affect their biological activity and promote changes in their photophysical behaviour. In particular, aggregation, axial ligation in metallo-porphyrins and protonation in free-base porphyrins induce alterations on their absorption spectra, fluorescence quantum yield, fluorescence lifetime and triplet state lifetime. TSPP was reported to form, under appropriate conditions of pH and ionic strength, highly ordered molecular aggregates of J-type [7,8]. This process of aggregation could be also induced when the porphyrin interacted with templates such as: micelles [9,10], vesicles [11] and proteins, namely, serum albumins (BSA and HSA) [12,13].

The stability of a protein in denaturing conditions (chaotropic agents, thermal effects, extreme pH) is of particular interest, since protein misfolding and aggregation may lead to the formation of amyloid fibrils or can be reflected in unbound drug concentration [14,15].

The unfolding pathway of serum albumins using urea or guanidine hydrochloride (Gdn-HCl) as denaturants is still a matter of controversy with conflicting results on the existence and nature of intermediate states. Some studies support the idea that unfolding of HSA occurs in a single step with no intermediates [16]. Others showed, using a multiple probe approach, that Gdn-HCl induced unfolding occurred through an incremental loss of structure but with no stable detectable intermediates [17]. The thesis that the unfolding of the albumin N isomer occurred through multiple steps with the presence of intermediates was supported by some authors [18–20]. Although a multistep unfolding pathway of HSA had been suggested for the process induced by urea, it seems likely that the opening sequence differs from that induced by Gdn-HCl [19].

In order to further elucidate this subject, we examined the unfolding behaviour of HSA in the presence of TSPP by chemical denaturation with Gdn-HCl. The heart-shaped 3-D structure adopted by HSA under physiological conditions (pH ~ 7, N-form) is composed of three homologous domains (I–III) further divided into subdomains A and B [21]. In spite of its size and complexity, HSA has a single tryptophan residue buried in the crevice of domain IIA whose sensitivity to local changes in the polarity of the medium makes it a useful fluorescent probe.

HSA conformation is strongly affected by changes in pH: at pH lower than 2.7, the protein adopts an extended conformation (E-form) with an extensive loss of the intra-domain helices of domain I and domain II and destruction of the local hydrophobic interactions between Trp^{214} and residues from domain IIIA [22]. Therefore, changes in the intrinsic fluorescence of HSA were followed as a function of denaturant concentration for protein and protein–porphyrin system at pH = 7 and pH = 2.5.

These data were complemented by UV–Vis extinction, induced CD, steady-state and transient-state fluorescence and fluorescence correlation measurements of TSPP bound to the protein to yield information on how ligand–protein interaction is affected under denaturation conditions.

In this paper we show that the non-covalent complex TSPP:HSA, besides contributing positively to the protein stabilization in the Gdn-HCl denaturation, can also report on protein structural changes occurring through a multistep unfolding process whereby HSA looses its structure incrementally during the denaturation process. These are relevant aspects to the investigation of drug biodistribution, since they will affect interactions with drug carrier proteins at its various folded states.

2. Experimental

2.1. Materials

HSA fraction V, 96–99% purity (catalogue no. A-1653) was purchased from Sigma and used without further purification. TSPP was obtained from Fluka ≥98% purity (catalogue no. 88074) and acrylamide 99% electrophoresis grade (catalogue no. 14,866-0) from Aldrich and both were used as received. Ultra pure guanidine hydrochloride (GdnHCl) from Fluka (catalogue no. 50933) was used without further purification. The probe concentrations were determined spectrophotometrically considering the molar extinction coefficient $\varepsilon^{HSA}_{280\,nm} = 42864\,M^{-1}\,cm^{-1}$ [23]; $\varepsilon^{TSPP}_{413\,nm} = 5.1 \times 10^5\,M^{-1}\,cm^{-1}$ at pH = 6 [24].

Buffer solutions were made up with bidistilled water, following the recommended procedures. In the pH = 2.5–7 range, a citrate-phosphate buffer (25 mM) was employed. All solvents were spectroscopic grade. In all experiments fresh stock solutions of protein and porphyrin in water were used.

2.2. Methods

Circular dichroism. CD spectra were obtained with a Jasco spectropolarimeter J-720 (Hachioji City, Tokyo) with spectral averaging and baseline correction. In the far-UV region the protein and TSPP concentrations were kept constant at 1.25 μM whereas 5 M was used for both in the visible region. The spectra (5–10 scans) were measured using 1 mm (for far-UV) and 10 mm (for visible) quartz cells and scanned at 20 nm/min, with a 0.2 nm step resolution and 1 nm bandwidth. The protein's CD signal (in mdeg) was converted to molar ellipticity $[\theta]$ (deg cm^2 dmol^{-1}) defined as $[\theta] = \theta_{obs}(10cl)^{-1}$, where θ_{obs} is the experimental ellipticity (mdeg), c (mol dm^{-3}) is the protein concentration, and l (cm) is the cell path length. Quartz cells were used and temperature was maintained at 24.0 ± 0.2 °C in a thermostated chamber by using a circulating water bath.

Extinction/absorption and steady-state fluorescence measurements. A Jasco V-560 spectrophotometer was employed in UV–Vis extinction measurements. Fluorescence measurements were recorded with a Perkin-Elmer LS 50B spectrofluorimeter, upon excitation at 297 nm to prevent excitation of tyrosine residues and therefore either emission or energy transfer to the indole side chain. The instrumental response at each wavelength was corrected by means of a curve obtained using appropriate fluorescence standards.

Time resolved fluorescence measurements. Fluorescence decays were obtained using the time-correlated single-photon counting (TC-SPC) technique with a Photon Technology International (PTI) instrument for tryptophan excitation at 295 nm [25]. A commercial equipment Microtime 200 from Picoquant GmbH was used for TSPP excitation. Here, the measurements are performed in front-face geometry and the backscattered light is attenuated through the use of appropriate filters. Excitation was achieved using a pulsed laser diode head at 405 nm with varied repetition rate (10, 20 or 40 MHz). The maximum output power is 0.4 mW and a minimum pulse width of 54 ps is obtained. A band-pass filter with a transmission in the range 600–800 nm was used to eliminate backscattered light in the photomultiplier tube from Picoquant (model PMA-182). Data acquisition can be recorded with 4096 channels per range with a time increment smaller than 40 ps. Data analysis was performed by a deconvolution method using a non-linear least-squares fitting program, based on the Marquardt algorithm. The goodness of the fit was evaluated by the usual statistical criteria and by visual inspection of the distribution of weighted residuals and the autocorrelation function.

Fluorescence correlation spectroscopy. FCS was performed in the same set-up. The 638 nm excitation light from a pulsed diode laser was focused by 60× water immersion objective with 1.2 NA, ~10 μm deep into the sample solution. Fluorescence was collected by the same microscope objective, passed through the dichroic mirror and appropriate band-pass filter (695AF55 Omega opti-

cal) and focused through a pinhole (75 μm), to reject out-of-focus light, onto a single-photon counting avalanche photodiode SPAD (Perkin-Elmer) whose signal was processed by TimeHarp 200 time-correlated single-photon counting card (PicoQuant). Focal area and detection volume were calibrated using Atto 655 dye in the carboxylic acid form (Atto-Tech GmbH, Germany) with known diffusion coefficient [26]. The increase of denaturant concentrations leads to changes in the viscosity and refractive index of the aqueous solutions which, in turn, introduces artifacts in FCS measurements preventing the correct definition of the detection volume or leading to artifacts in diffusion components. This problem was minimized by using a small pinhole aperture [27]. To minimize aberrations due to refractive index mismatch, the correction collar and the objective position were systematically tested in order to provide the best conditions for FCS measurements at each Gdn-HCl concentration [28]. Data analysis of individual correlation curves was performed using SymPhoTime (PicoQuant) and a programmed global fitting analysis was carried out in MS Excel.

2.3. Data analysis

Unfolding equilibrium studies: chemical unfolding by Gdn-HCl—A stock solution of Gdn-HCl was prepared by diluting the proper amount of powder in the desired buffer. Due to the high hygroscopy of the denaturant the accurate concentration of the final solution (~8 M) was determined using the relationship between the refractive index and the concentration of Gdn-HCl [29]. Chemical denaturation was carried out at 25 °C at pH = 2.5 and 7, with 1.50 mL of a given protein or protein–porphyrin solution. The latter was prepared *ca.* 1 h prior to initiate the unfolding assays due to the aggregation kinetics of TSPP. Titration was carried out by adding aliquots of the denaturant stock solution to a given solution ([HSA] = 5 μM was kept constant and [TSPP] varied from 0 to 10 μM) under constant stirring and left to equilibrate (which was achieved in about 10 min). The spectra obtained were corrected for blank and dilution contributions. Unfolding curves normalized to the maximum were obtained by integrating the fluorescence spectra in the 300–500 nm wavelength range, and were analyzed assuming a two-state transition from the native state (N) to the unfolded state (U). Taking Y as the observed variable parameter, Y_N and Y_U are the characteristic values of the protein molecules in the respective states, f_U and f_N represent the relative protein fractions calculated as follows:

$$f_U = \frac{Y - Y_N}{Y_U - Y_N} \quad \text{and} \quad f_N + f_U = 1 \tag{1}$$

Then the difference in free energy between folded and unfolded states, G_{un}, and the unfolding equilibrium constant, K_{un}, are given by:

$$\Delta G_{un} = -RT \ln K_{un} = -RT \ln \left(\frac{f_U}{f_N}\right) = -RT \ln \left[\frac{Y - Y_N}{Y_U - Y}\right] \tag{2}$$

ΔG_{un} depends linearly on the denaturant concentration [D], making the linear extrapolation model the most used procedure to obtain $\Delta G_{un}^{H_2O}$, the free energy change for the unfolding reaction in the absence of denaturant, expressed as [29]

$$\Delta G_{un} = \Delta G_{un}^{H_2O} - m[D] \tag{3}$$

where m is a constant of proportionality and hence, the denaturant concentration at which half of the protein molecules are unfolded, $D_{1/2}$, can be obtained by $D_{1/2} = \Delta G_{un}^{H_2O}/m$. In the fittings, pre- and post-unfolding baselines were assumed because the spectroscopic signals of each state change linearly with [D]. The analysis of the unfolding profiles was performed by combining the baseline slopes with Eqs. (2) and (3) into the following equation [30]:

$$Y = \frac{Y_{0N} + m_N[D] + (Y_{0U} + m_U[D])e^{-(\Delta G_{un}^{H_2O} - m[D])/RT}}{1 + e^{-(\Delta G_{un}^{H_2O} - m[D])/RT}} \tag{4}$$

where Y_{0N} and Y_{0U} are the signals extrapolated to zero denaturant concentration for the native and unfolded states, respectively; m_N and m_U are the slopes for the dependencies of Y_{0N} and Y_{0U} on [D]. The errors of calculated parameters were accessed using the error propagation theory and the distribution F of Snedcor was used to confirm with 99% of confidence the relationship among the variables [31].

Determination of translational diffusion coefficients by FCS: Diluted porphyrin samples were investigated by FCS. The intensity fluctuations caused by the variation of the number of fluorescent molecules diffusing in and out the confocal sample volume were analyzed by the normalized temporal autocorrelation function $G(\tau)$ as a function of the correlation time τ. The transition to the triplet state can also lead to fluctuations in intensity since the molecule needs a comparably long time to relax back to the ground state and since it cannot emit during these intervals appears dark. Assuming a three dimensional Gaussian sample volume with a $1/e^2$ axial (z_0) to lateral (w_0) dimension ratio k ($k = z_0/w_0$), the full correlation curve describing translational diffusion of a fluorescent species and a common triplet term is then given by Eq. (5) provided that $\tau_D \gg \tau_T$:

$$G_{DT}(\tau) = \frac{1}{N}\left(1 + \frac{\tau}{\tau_D}\right)^{-1}\left(1 + \frac{\tau}{k^2\tau_D}\right)^{-1/2}(1 + Te^{-\tau/\tau_T}) \tag{5}$$

where N and τ_D are, respectively, the mean number of fluorescent molecules and the characteristic diffusion time for a molecule through the sample volume. τ_D is related to the translational diffusion coefficient D by $D = w_0^2/4\tau_D$, T is the fraction of molecules in the triplet state and τ_T is the triplet state conversion time. After-pulsing artifacts visible at the onset of the FCS curves were purged by performing FLCS analysis with the software provided (SymPhoTime, PicoQuant). The temperature of the experiments was stabilized at 22 °C.

3. Results

Based on spectroscopic data, we have previously shown that TSPP binded to albumins at both pH = 7 and pH = 2.5 with relatively high binding constants ($K_B \sim 3$–$5.10^6\ M^{-1}$), where electrostatic and hydrophobic interactions were involved [13]. Moreover, under acidic conditions where TSPP was prevalently present in solution as a zwitterion, the formation of highly ordered molecular aggregates of the porphyrin at relatively low [TSPP] were induced [13,32].

In turn, the presence of increasing amounts of TSPP resulted in saturate, concentration-dependent quenching of the Trp^{214} fluorescence in HSA and put into evidence a mechanism of efficient energy transfer from the amino acid to the porphyrin. The value obtained, $R_0 \approx 56$ Å [33] suggested a long-distance Forster-type resonance energy transfer but did not let us distinguish between any of HSA binding sites. We now present data concerning the chemical unfolding of HSA in the presence of TSPP at different pH, following the protein intrinsic fluorescence which indicates that in these conditions the energy transfer process is inhibited.

3.1. HSA unfolding followed by the intrinsic fluorescence of Trp^{214}

pH = 7—Chemical denaturation of HSA–TSPP following Trp^{214} fluorescence resulted in a different curve from that of native protein ([HSA] = 5 μM), Fig. 1A. The pre-unfolding baseline, *i.e.*, the linear dependence of native protein fluorescence on the denaturant concentration before the transition, went up to 1.8 M which was characterized by a 20% increase in the integrated area and a

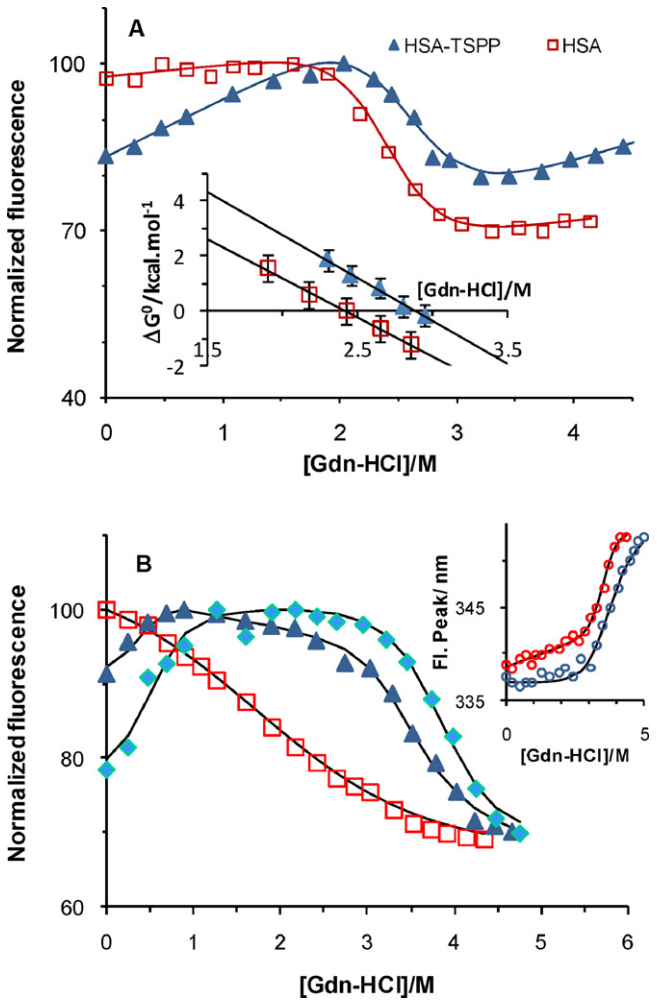

Fig. 1. Gdn-HCl induced unfolding curves of HSA–TSPP and HSA monitored by integrated fluorescence intensity of Trp^{214} in HSA (□), and in the presence of different HSA–TSPP ratios (▲, 1:0.4); (◆, 1:1), at pH = 7 (A) and pH = 2.5 (B). Inset (A): Dependence of free energy change on [Gdn-HCl] for the transitions showed. Inset (B): Dependence of fluorescence peak of Trp^{214} in HSA (○) and on HSA–TSPP (○) on [Gdn-HCl] at pH = 2.5. λ_{exc} = 297 nm. ([HSA] = 5 μM). (For interpretation of the references to color in this figure legend, the reader is referred to the web version of the article.)

2-nm blue shift in the fluorescence peak. The main unfolding transition occurred between 1.8 M and 3 M of denaturant with a 35% decrease in intensity together with a 15-nm red shift in the fluorescence peak. Free energies and *m*, obtained with and without TSPP are not sufficiently different (inset Fig. 1A and Table 1) to assume that more residues were involved in the solvent exposure of HSA [34].

Table 1
Thermodynamic parameters of Gdn-HCl induced unfolding transitions of HSA (5 μM) in the presence of different [TSPP] by monitoring changes in Trp^{214} fluorescence intensity at pH = 7 and 2.5, analyzed using Eq. (4).

pH	[TSPP] (μM)	$\Delta G_{un}^{H_2O}$ (kcal mol^{-1})	*m* (kcal mol^{-1} M^{-1})	$D_{1/2}$ (M)
7	0	7.0 ± 1.1	2.8 ± 0.2	2.5 ± 0.1
	2	9.1 ± 1.1	3.1 ± 0.2	2.9 ± 0.1
2.5	0	*n.d.* (6.2 ± 1.3)[a]	*n.d.* (1.8 ± 0.3)[a]	*n.d.* (3.4 ± 0.3)[a]
	2	6.8 ± 1.1	2.0 ± 0.2	3.4 ± 0.2
	5	9.3 ± 1.1	2.4 ± 0.3	3.9 ± 0.2
	10	7.2 ± 1.0	2.1 ± 0.3	3.4 ± 0.2

n.d.: not defined.
[a] Obtained from changes in Trp^{214} fluorescence peak (nm).

At high denaturant concentrations, the intensities became comparable, which suggested that the protein reached similar opened forms irrespective of TSPP presence. At this stage, the fluorescence signal of the latter is not influenced by TSPP presence at [Gdn-HCl] above 3 M indicating that TSPP no longer interacts with Trp^{214}.

pH = 2.5—The Gdn-HCl profile of integrated fluorescence intensity obtained for native HSA (5 μM) under acidic conditions showed a continuous non-cooperative process (Fig. 1B). However, the dependence of emission wavelength peak on the denaturant concentration showed that the major changes (64%) occurred between 2.8 and 4 M of Gdn-HCl (inset Fig. 1B). Curiously, in the presence of TSPP (5 μM) two main transitions were detected from intrinsic tryptophan fluorescence upon denaturant addition. The first one, took place at low concentrations of denaturant 0 < [Gdn-HCl] < 1 M and, in general, led to an increase in Trp^{214} fluorescence intensity, without wavelength shift, not detected in samples without TSPP. This can be taken as an indication of changes in the proximity of quencher groups to Trp: the porphyrin itself or nearby amino acids with side chains able to quench Trp fluorescence by excited-state electron transfer (*e.g.* histidine, asparagine, cysteine glutamic and aspartic acid) or by excited-state proton transfer (*e.g.* lysine and tyrosine). On the other hand, fluorescence recovery of Trp^{214} under these mild denaturant conditions depended on the amount of TSPP, being more important as [TSPP] increased.

The second transition occured at 3 ≤ [Gdn-HCl] < 4 M with a significant decrease inTrp^{214} fluorescence intensity and more than 12 nm red-shift, characteristic of Trp exposure to a polar environment. The process was more cooperative in the presence of the porphyrin, taking into account the fact that the jump in the transition between the two states was steeper in the porphyrin's presence. The latter also contributed to a shift of the transition mid-points to higher denaturant concentrations being maximal at a molar ratio protein/porphyrin of 1.

The accessibility of acrylamide (AA) to both the native and denatured forms of the protein in the presence of increasing amounts of TSPP was also assessed (see Supporting Information, Fig. S1). Acrylamide is known to effectively quench Trp fluorescence by an electron transfer mechanism which is sensitive to exposure of such residues. Data concerning the aqueous solution of each protein has already been published. An upward curvature in the Stern–Volmer plot has been identified with the existence of static contributions accounted for by a quenching active sphere volume [13]. TSPP affected both dynamic and static quenching processes of native HSA, at pH = 2.5: until up to [TSPP] ~ 5 M, the dynamic process was less effective than without TSPP, whereas above that value the process was reversed and the efficiency became even greater than without TSPP. Nevertheless, without Gdn-HCl, the presence of TSPP did not lead to drastic variations in k_q (less than 22%).

The values of k_q obtained upon addition of 5.5 M Gdn-HCl denoted a sharp increase in the exposure of Trp^{214} (Fig. S1). TSPP concentrations below 10 μM, seemed to induce a certain degree of structural alterations, taking into account the reduced accessibility of Trp^{214} to AA. This was consistent with the increase of $D_{1/2}$ obtained in this [TSPP] range (Table 1). However, this stabilization is lost at higher [TSPP] where k_q increases *ca.* 30%. Therefore, it is likely that some residual structure is still present in the protein even after incubation with 5.5 M Gdn-HCl, probably due to the presence of disulfide bonds in the protein which hold different parts of the polypeptide covalently connected.

3.2. Far-UV circular dichroism

HSA—Conformational variations affecting the secondary structure of HSA were monitored by far-UV CD at pH = 2.5 and 7. The CD spectra obtained at different denaturant concentrations presented no isodichroic points, Fig. 2A. As expected, the absolute values of

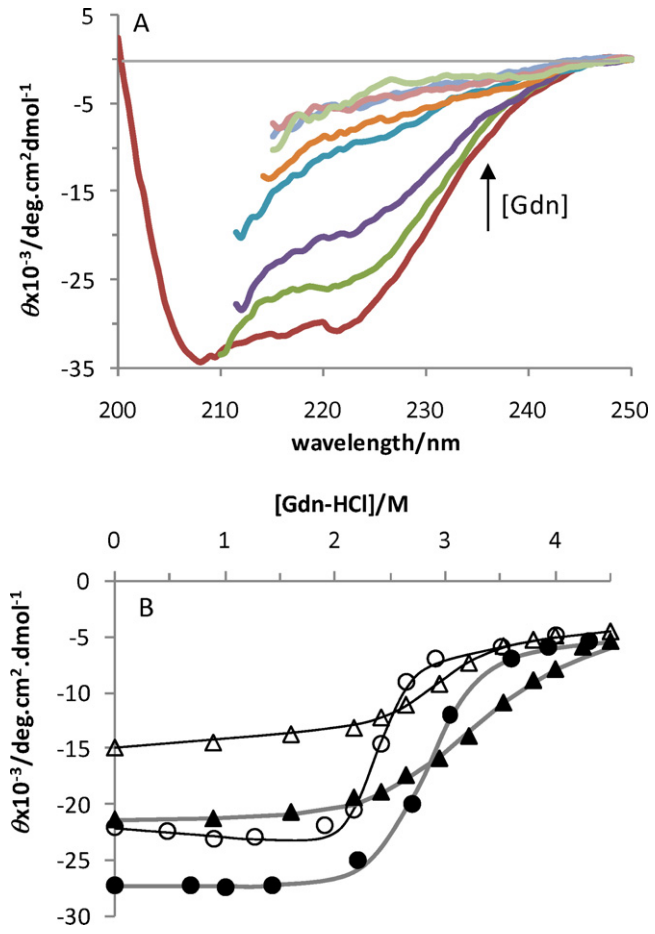

Fig. 2. (A) Far-UV CD spectra of HSA–TSPP complex at pH = 7 in the presence of increasing [Gdn-HCl]: 0–4 M; (B) dependence on denaturant concentration of the CD signal obtained at 222 nm: HSA at pH = 2.5 (△), HSA at pH = 7 (○), HSA–TSPP complex at pH = 2.5 (▲), and at pH = 7 (●). ([HSA]/[TSPP] = 1; [HSA] = 1.25 μM).

CD decreased upon protein denaturation giving evidence to the loss of the secondary structure. The changes obtained in the CD signal at 222 nm, Fig. 2B, showed a more cooperative process for the unfolding of HSA at pH = 7 (with a transition midpoint concentration $D_{1/2} = 2.4 \pm 0.1$ M) than to that at pH = 2.5, similar to what was detected through Trp^{214} fluorescence.

In turn, at acidic pH, even in the absence of Gdn-HCl, there was considerably less native secondary structure. Taken together, these data seemed to support the hypothesis of a molten globule-like state previously assigned to the E-form [35]. This form refers to a compact state with few tertiary interactions, some secondary structure and a fluctuating hydrophobic core [34]. The term was used here in a broad sense since various molten globule-like states with different degrees of structural organization had been previously revealed.

The denaturation profile for the E-form showed a transition midpoint concentration $D_{1/2} = 2.9 \pm 0.2$ M.

HSA/TSPP—Upon addition of TSPP on a 1:1 molar ratio at both pH studied and in the absence of denaturant, there was an increase in the absolute value of CD (Fig. 2A and B). This can be translated as an increase in α-helix content from 58% to 66% (obtained using the equation described by [36]) and similar to what was reported before for the BSA–TSPP system [37]. Therefore, this represents a state distinct from that without TSPP, but still falling within the concept of a molten globule-like state. In this case, there was a shift in the denaturation conditions towards higher [Gdn-HCl], Table 1.

3.3. HSA unfolding followed by bound TSPP extinction and fluorescence

pH = 7—Unfolding curves were also obtained from TSPP (2 μM) extinction and fluorescence changes upon increasing additions of Gdn-HCl and [HSA] = 2 μM, Fig. 3. Three distinct regions can be defined which were compared with data for TSPP in the absence of the protein. The 1st stage occurred until up to 1 M Gdn-HCl which was characterized by a 25% decrease in Soret band absorbance together with a 6-nm blue shift (Fig. 3A), and a less pronounced blue shift (2 nm) with almost 40% decrease in fluorescence intensity (Fig. 3D). Taking into account that TSPP fluorescence loss took place in the same denaturant concentration range as Trp^{214} fluorescence increased (see Fig. 1), it is feasible that the process of FRET from Trp^{214} to TSPP, mentioned above, is being affected under these conditions. Nonetheless, it did not account for the all fluorescence loss. Changes in TSPP extinction were consistent with the formation of aggregated species which also contributed to the decrease of TSPP fluorescence intensity.

In the 2nd stage, 1 M < [Gdn-HCl] < 3 M, the spectroscopic data was reversed: an almost 50% increase in absorbance together with a red shift almost reached again the value of TSPP bound to HSA in the absence of denaturant (Fig. 3B). These changes occurred in parallel with those reported by Trp^{214} in domain II.

A 3rd stage took place at [Gdn-HCl] > 3 M, characterized by another drop in absorbance typical of the HSA–TSPP complex (@422 nm, Fig. 3C) and in fluorescence intensity (□, Fig. 3F), to values similar to those in the absence of protein for the same high denaturant concentrations. On the other hand, a transition with a concentration mid-point ~3.7 M of Gdn-HCl could be followed @415 nm (■, Fig. 3E) which reflected the presence of free monomeric TSPP in aqueous solution. Nevertheless, the absorption maximum showed a 4 nm red-shift comparatively to the one obtained for the tetra-anion monomers free in water at neutral pH. This shift may reflect changes in the physicochemical properties of the aqueous solution (namely, increase of refractive index) due to the high denaturant concentrations. The electronic spectra of centrosymmetric molecules like porphyrins are normally correlated with the function $f(n^2) = (n^2 - 1)/(2n^2 + 1)$, which means that induced polarization and dispersion forces are mainly responsible for the spectral shift observed in these molecules [38]. In fact, in the absence of HSA, the shifts of the TSPP Soret band peak followed a linear trend with $f(n^2)$ (Fig. S2). On the other hand, it is known that specific interactions between guanidine and the sulfonate groups of TSPP may also take place, which include a salt bridge, ion-dipole and hydrogen bonding interactions [39], contributing as well to the spectral shift.

pH = 2.5—Under acidic conditions, and depending on the concentrations of both protein and porphyrin, the latter can exist in distinct forms which can be differentiated by spectral parameters or fluorescence lifetimes. In this context, we have followed changes in absorbance at characteristic wavelengths: 435 nm, corresponding to monomeric di-acid species in solution; 490 nm usually associated to J-aggregated porphyrin at the protein surface [10,13]; and 422 nm assigned to neutral monomers associated with the protein (Fig. 4).

The addition of low amounts of Gdn-HCl (≤1 M) led to significant changes in TSPP extinction and fluorescence, namely, a decrease in OD@422 nm and in TSPP fluorescence intensity (inset Fig. 4A, □). Simultaneously, an increase was found in OD@490 nm (inset Fig. 4A, ○) which is partially due to changes in the ionic strength of the solution thus stabilizing J-aggregates [32,40]. This fact may also contribute to a drop in TSPP fluorescence since J-aggregates are known to have a much lower fluorescence quantum yield [41].

In the concentration range 2.5 < [Gdn-HCl] < 4 M, a second transition was observed in the absorbance of TSPP which showed that

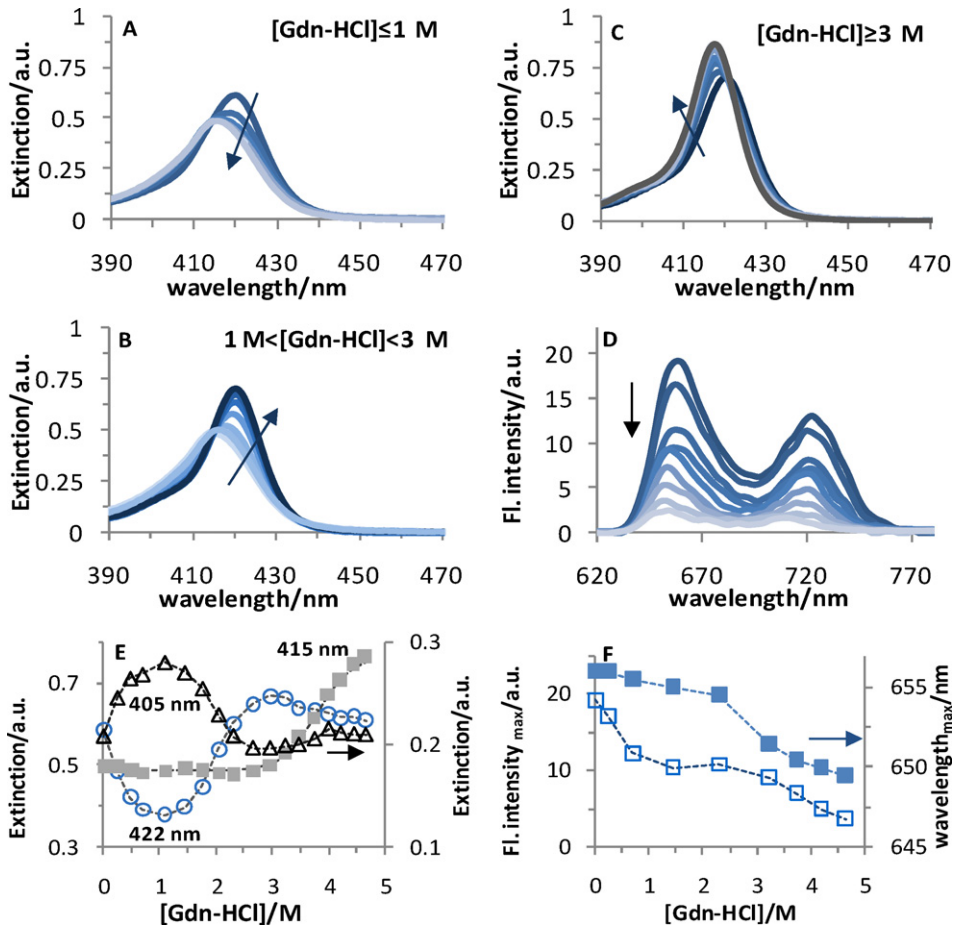

Fig. 3. Spectral changes in Soret band extinction (A–C) represent the three different sets of [Gdn-HCl]; the last spectrum of each plot is the first of the next plot) and in fluorescence intensity (D) of TSPP–HSA complex upon addition of Gdn-HCl, at pH = 7. (E) Dependence of TSPP–HSA extinction at 405 nm (△); 415 nm (■); and at 422 nm (○) on [Gdn-HCl]. (F) Dependence of TSPP–HSA fluorescence intensity (□) and wavelength maximum (■) on [Gdn-HCl]. ([HSA] = [TSPP] = 2 μM, λ_{exc} = 400 nm; arrows indicate the increase of [Gdn-HCl]). (For interpretation of the references to color in this figure legend, the reader is referred to the web version of the article.)

J-aggregates were clearly destabilized. The Gdn-HCl concentration at which it happened depended on the amount of TSPP present, increasing as [TSPP] increased for a constant [HSA], as expected. The Soret band peak of absorbance was exactly the same with or without HSA at high [Gdn-HCl], i.e., 443 nm (Fig. S3). This represented a 10 nm red-shift relatively to the di-acid monomers in aqueous solutions, as already observed for the tetra-anionic monomers at pH = 7.

At [Gdn-HCl] above which J-aggregation was destabilized (>2.5–3 M depending on [TSPP]) there was a notorious increase in

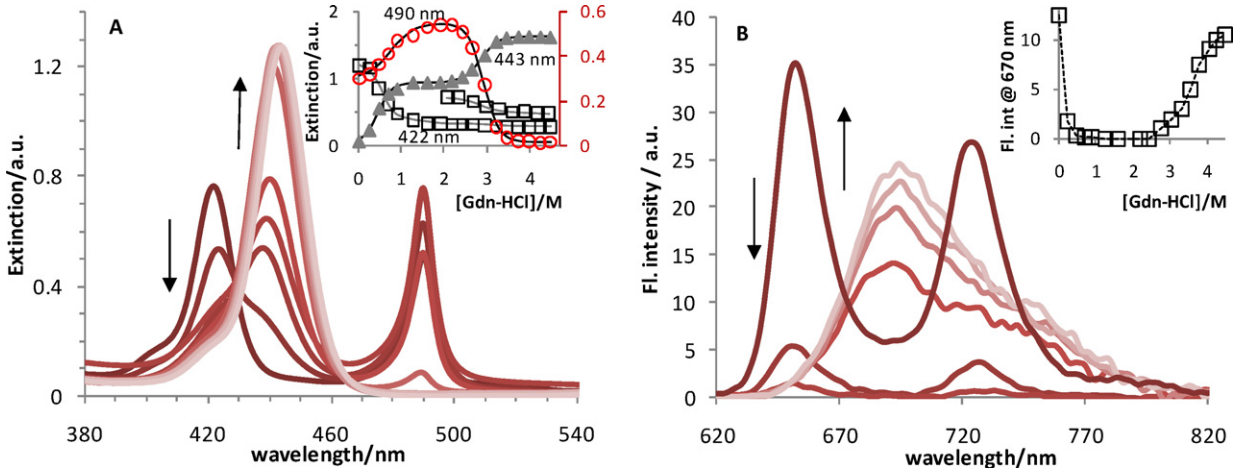

Fig. 4. Spectral changes in Soret band absorption (A) and in fluorescence intensity (B) of TSPP–HSA complex upon addition of Gdn-HCl at pH = 2.5. Inset (A): Dependence of TSPP–HSA absorbance at 422 (□ scaled up at high denaturant concentrations), 443 nm (▲) and 490 nm (○) on [Gdn-HCl]. Inset (B): Dependence of TSPP–HSA fluorescence intensity at 670 nm (□) on [Gdn-HCl]. ([HSA] = [TSPP] = 2 μM; λ_{exc} = 405 nm; arrows indicate the increase of [Gdn-HCl]). (For interpretation of the references to color in this figure legend, the reader is referred to the web version of the article.)

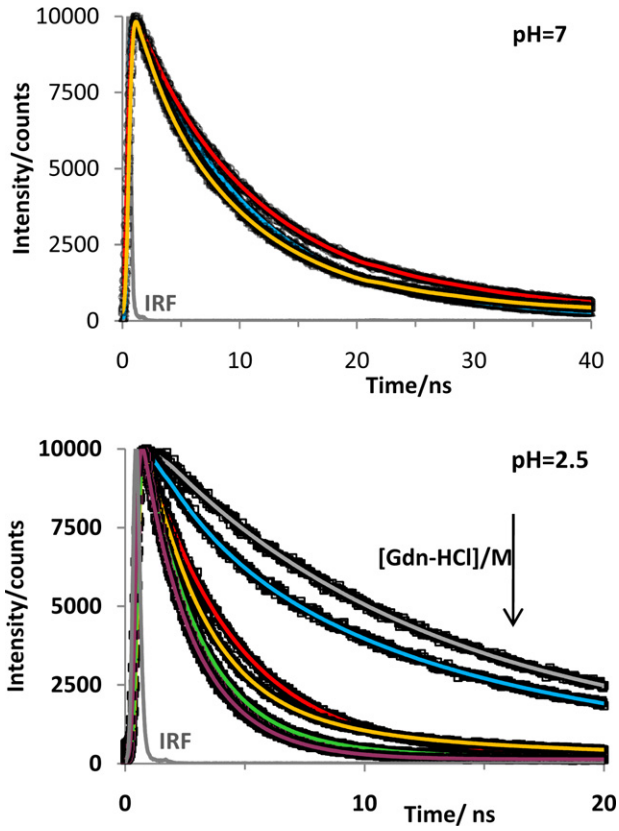

Fig. 5. Fluorescence decays of TSPP–HSA (1:1 ratio) at pH = 7 and pH = 2.5, as a function of [Gdn-HCl]: 0–5 M.

the porphyrin fluorescence intensity. The former two band-shape characteristic of TSPP–HSA complex was replaced by a single band indicative of the monomeric di-acid species, the latter being red-shifted relatively to that of aqueous solution in line with absorbance data showed above.

3.4. Time-resolved fluorescence measurements

The fluorescence decays of TSPP are sensitive, among other factors, to the degree of porphyrin association to HSA and to the protonation state of pyrrolic nitrogens [13]. In the absence of the protein, emission decays showed a biexponential behaviour with characteristic lifetimes for the monomeric di-acid species of ~3.75 ns (pH = 2.5) and of 9.78 ns for the tetra-anionic one (pH = 7), Fig. 5. In the presence of HSA, the fluorescence decays were dominated by a long lifetime component of ~12 ns regardless of the solution pH (Table 2) indicative of the porphyrin binding

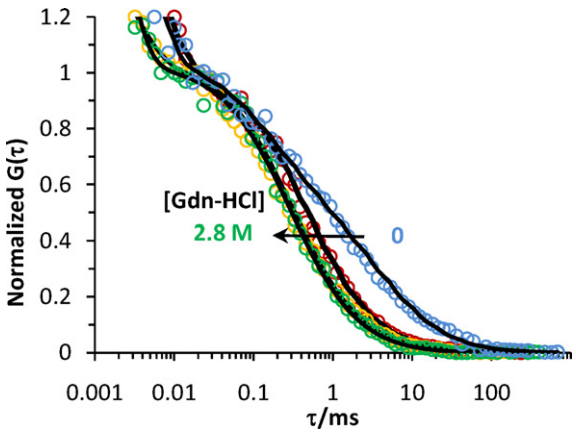

Fig. 6. Normalized autocorrelation curves of TSPP–HSA (1:1 ratio) at pH = 7 measured with increasing [Gdn-HCl]: 0 (blue); 1.8 M (red); 2.8 M (yellow) and without HSA (green). ([TSPP] = 0.7 μM). (For interpretation of the references to color in this figure legend, the reader is referred to the web version of the article.)

in the protein interior. This value was similar to those reported for both the di- and tetra-anion TSPP in Triton X-100 micelles [9]. Another similarity with the micellar system could be established for TSPP/HSA with 1 M Gdn-HCl at pH = 7, where an intermediate lifetime (~1.5 ns) was also obtained and previously assigned to the existence of aggregates [9]. The long-component contribution decreased rapidly with denaturant addition and above ~2 M Gdn-HCl it was no longer detected at either pHs. Instead, two shorter lifetimes were obtained which coincided with those retrieved for TSPP in the absence of protein at the same denaturant concentrations. Due to changes in the solution refractive index caused by the Gdn-HCl addition, the monomer lifetime decreased at both pHs. Under these conditions, TSPP was free in solution and monomers coexisted with small aggregates (most probably, dimers) which would account for the sub-nanosecond component. The similarity of the shorter component obtained at pH = 7.4 and that of the di-anion monomer did not allow us to disregard the possibility of a slight pH drop at very high denaturant concentrations.

3.5. Fluorescence correlation spectroscopy

FCS has been successfully used to monitor changes in diffusion coefficients in biological systems due to the high sensitivity and the wide timescales covered [42]. The diffusion coefficients of a free probe or a probe bound to a protein should be distinct enough to be accurately determined by FCS measurements [43]. The normalized fluorescence intensity correlation curves $G(\tau)$ of TSPP–HSA in aqueous solution (pH = 7.4) at different denaturant concentrations are shown in Fig. 6. The correlation function obtained for TSPP–HSA in the presence and absence of Gdn-HCl was fitted to

Table 2
Fluorescence lifetimes of TSPP in aqueous buffer solution in the presence of HSA (1:1 ratio), with and without Gdn-HCl (λ_{exc} = 405 nm; λ_{emi} = 600–800 nm; $\Delta\tau_i$ = 3%; χ^2 < 1.2).

pH	Sample	A_1 (%)	τ_1 (ns)	A_2 (%)	τ_2 (ns)	A_3 (%)	τ_3 (ns)
7	TSPP	89	9.781	11	0.418	–	–
	TSPP/HSA	10	9.804	13	0.305	77	11.85
	TSPP/HSA + 1 M Gdn	37	9.280	44	1.554	19	12.01
	TSPP/HSA + 5 M Gdn	90	8.751	10	2.130	–	–
2.5	TSPP	90	3.750	10	0.198	–	–
	TSPP/HSA	5.3	3.600	–	–	94.7	11.98
	TSPP/HSA + 0.5 M Gdn	28	3.571	–	–	72	11.90
	TSPP/HSA + 1.25 M Gdn	86	2.810	–	–	14	11.59
	TSPP/HSA + 1.8 M Gdn	96	2.510	–	–	4.0	11.37
	TSPP/HSA + 2.8 M Gdn	85	2.430	15	0.659	–	–
	TSPP/HSA + 3.8 M Gdn	86	2.331	14	0.623	–	–
	TSPP/HSA + 5 M Gdn	78	2.279	22	0.609	–	–

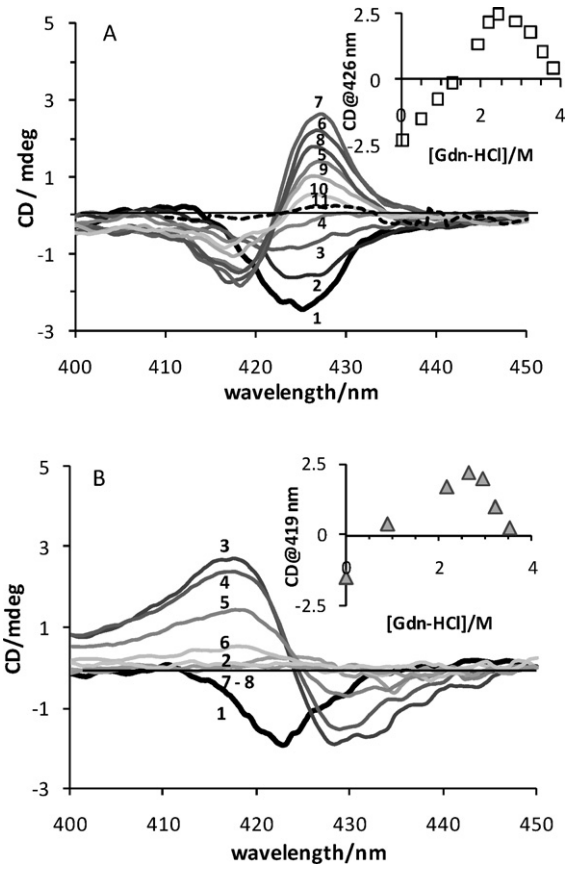

Fig. 7. Induced CD spectra of TSPP–HSA (1:1 ratio) at (A) pH = 7 and at (B) pH = 2.5, in the presence of different [Gdn-HCl], 0–3.8 M. Inset: Dependence of induced CD at 422 nm of TSPP–HSA on [Gdn-HCl] at (A) pH = 7 and (B) pH = 2.5. ([HSA] = [TSPP] = 2 μM).

Eq. (5). The triplet term $\tau_T \approx 1\,\mu s$ presented a significant contribution $T \approx 50\%$, under all experimental conditions. The diffusion time obtained for TSPP–HSA without denaturant ($\tau_D = 477 \pm 35\,\mu s$, corresponding to a diffusion coefficient, $D = 0.54 \times 10^{-10}\,m^2\,s^{-1}$) shifted to shorter correlation times upon addition of Gdn-HCl. At the higher concentration of Gdn-HCl tested (2.8 M), the autocorrelation curve perfectly superimposes that of free TSPP at the same pH and Gdn-HCl concentration. The diffusion coefficient obtained from the fit, $D = 2.2 \pm 0.3 \times 10^{-10}\,m^2\,s^{-1}$, was related to the apparent hydrodynamic radius (R_H) by the Stokes-Einstein relationship $D = kT/6\pi\eta R_H$. The value of $R_H = 9.0 \pm 0.3$ Å agreed with previous findings and pointed to the prevalence of free porphyrin already at 2.8 M Gdn-HCl as fluorescence decays analysis already suggested. A similar picture was obtained for pH = 2.5 (data not shown).

3.6. Induced visible circular dichroism in TSPP–HSA complex

TSPP itself does not have a CD signal in the UV–Vis range as expected for an achiral molecule. Nonetheless, an induced CD signal was detected in the visible range upon binding to HSA arising from the chiral environment provided by the protein binding sites. We followed the CD signal in this region upon addition of Gdn-HCl, Fig. 7. It is worth mentioning that no induced CD was detected in the absence of the protein, *i.e.*, for the TSPP/Gdn-HCl system. However, at both pH = 2.5 and pH = 7, in the presence of equimolar ratios of HSA/TSPP ([TSPP] = 2 μM), a low intensity single trough was detected at ~424 nm, indicative of induced CD and with maximum in line with that obtained by extinction. At neutral pH, the initial single band decreased upon denaturant addition up to ~1.5 M, above which a bisignate signal CD was observed corresponding to a positive Cotton effect, Fig. 7A. Under acidic pH conditions, initial additions of denaturant ([Gdn-HCl] ≤ 1 M) led to a decrease in the CD signal, which changed after further addition of denaturant to a bisignate CD signal corresponding to a negative Cotton effect, Fig. 7B. The bisignate signal in the visible region of the spectrum was also detected when J-aggregates predominate over the protein–TSPP complex [13]. As pointed out above, there is a stabilization of J-aggregates upon the initial additions of denaturant which coincides with the prevalence of the bisignate CD signal. This signal reached its maximum at [Gdn-HCl] = 2.7 M, tending to zero on further increasing the denaturant concentration thus, confirming that TSPP has been completely released into the aqueous solution at *ca.* 4.0 M Gdn-HCl.

4. Discussion

In this work we dedicated our attention to the denaturing effects of Gdn-HCl on HSA in the presence of TSPP as well as to pH effects. Although the physiological pH = 7 has more interest in studies related to proteins, some striking features of TSPP–HSA association occur in acidic conditions and are useful as a means to obtain information regarding the protein response to changes in local environment.

4.1. TSPP binding effects on HSA stability towards unfolding

In the presence of TSPP, there were substantial changes in the Gdn-HCl induced unfolding profile of HSA: (i) an increase in the process cooperativity at pH = 2.5 and (ii) a shift in the unfolding transition towards higher denaturant concentrations at both pH studied.

Even in the absence of denaturant, we found that TSPP presence led to an increase in the protein ellipticity at 222 nm (Fig. 2B), *i.e.*, promoted a richer α-helix structure. Using BSA, we were able to show that the diffusional as well as the rotational motions of BSA–TSPP (1:1) complex at pH = 7.4 were similar to those of the free native protein [37]. Conversely, at pH = 2.5 faster diffusional and rotational times were obtained for the BSA–TSPP complex. Being an anionic species (global charge = −4 at pH = 7 and −2 at pH = 2.5), TSPP can interact electrostatically with the protein cationic sites providing a shielding effect on the repulsive positive charges, particularly relevant under acidic conditions. Combining this information, we propose a more compact structure (E_c in Scheme 1) for the HSA–TSPP complex at pH = 2.5. These changes may also involve Trp, since a slight decrease in the degree of exposure to acrylamide is inferred from k_q decrease for the 1:1 HSA–TSPP complex (Supporting Information).

This ligand-induced compact structure of HSA at low pH seems to enhance further the protein stability towards environmental changes: there is a stabilization of Trp environment towards unfolding by Gdn-HCl with [TSPP] which occurs above 3 M, as indicated by the $D_{1/2}$ values. A trade-off between structural stability and function has been proposed for HSA to explain the adaptability and flexibility of drug site 2 in domain III in opposition to a more rigid binding site of domain I [44]. The ligand capability to reduce the protein flexibility was also highlighted in the thermal stabilization of BSA by 1,8-ANS previously reported [45] together with the relevance of electrostatic interactions to the binding. In line with these findings, also cyanocobalamine (vitamin B12) was reported to induce the increase of α-helix content of HSA upon binding to its surface [46], where electrostatic effects were also prevalent. Conversely, the binding of a porphyrin similar to TSPP in which the sulfonato groups are replaced by hydroxyl ones (THPP), was reported to cause a reduction in HSA α-helix structure leading to a more loose tertiary structure [47]. It was suggested that the main

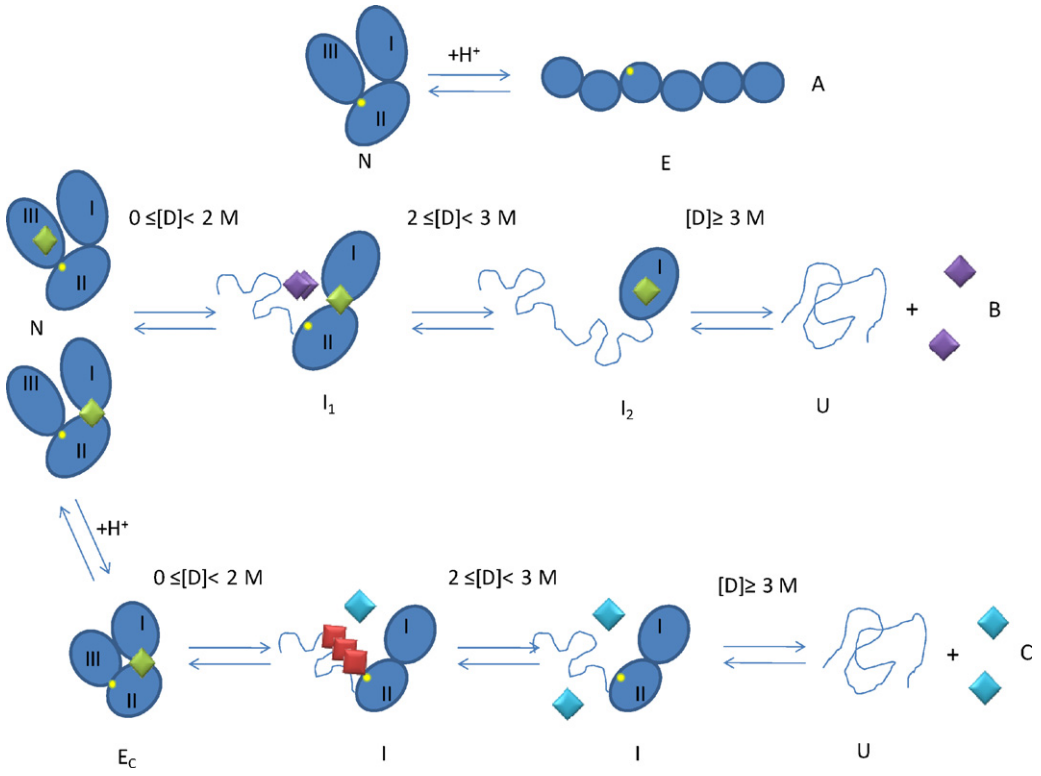

Scheme 1. Schematic representation of the (A) conformational transitions from neutral form –N, at pH = 7 to the extended form –E, at pH = 2.5; and of the mechanism of Gdn-HCl induced unfolding of HSA at pH = 7 (B) and pH = 2.5 (C). The protein domains are represented in dark blue in which the yellow dot represents Trp^{214} in subdomain IIA. The lozenges represent the porphyrin in different states: monomer associated to HSA (green), J-aggregates at the protein surface (red), H-aggregates or free tetra-anion in neutral solution (purple), and free di-anion in acidic solution (light blue). The letters indicate HSA prevalent conformational structure: N (native HSA, pH = 7); E_c ("compact structure", pH = 2.5); I, I_1 and I_2 (intermediates) and U (unfolded HSA). (For interpretation of the references to color in this scheme legend, the reader is referred to the web version of the article.)

driving force is hydrophobic in nature and molecular modelling pointed to the porphryin being partially accommodated in subdomain IIIA. Competitive binding studies of chlorine P6 and purpurin 18 to HSA pointed to the location of these photosensitizers in the warfarin binding site (domain II) causing little change in the secondary structure of the protein [48]. Hence, it could be speculated that the nature of the interaction involved in ligand–protein binding determines the ligand location in the protein structure which in turn may either become compacted or loose.

The next step is to try to relate the changes reported by TSPP and HSA signals with the unfolding of the different domains in HSA in order to clarify the porphyrin binding site(s). Our previous findings involving TSPP binding to HSA under native conditions, provided evidence for different locations of TSPP, namely the hydrophobic pockets of the various domains with analogous affinity, confirmed by FRET results which did not exclude any of HSA binding sites [13]. The fluorescence enhancement registered for Trp^{214} in the presence of low amounts of Gdn-HCl (<2 M) with the simultaneous drop in TSPP fluorescence suggests the FRET process between these two fluorophores is affected by the denaturant addition. Since the process efficiency depends, among other aspects, on the distance between the donor and the acceptor and their reciprocal orientation, Gdn-HCl may impose alterations in HSA domains which contribute to changes in these parameters.

The fluorescence of Trp^{214} is very sensitive to changes in its microenvironment and since no shift was detected in this emission within the denaturant concentration range we may conclude that sub-domain IIA is not affected at this stage.

On the other hand, it was reported in the HSA–acrylodan system a decrease in the quenching efficiency by acrylodan (located in domain I) at [Gdn-HCl] ~ 2 M [18,49] and assigned to the separation of domains I and II. This interdomain separation also contributed to the loss of high affinity binding sites of palmitic acid (located at the interface of domains I and II) at low [Gdn-HCl], while those low affinity sites located in the interior of domain II remained unaffected [17]. The binding of diazepam to HSA (in domain III [21]) was completely lost around 1.4 M Gdn-HCl, thus being reported as the most labile domain towards chemical denaturation [50].

Therefore, the first changes in TSPP signals could report the loss of binding site in domain III and/or the separation of domains I and II. Data obtained at higher denaturant concentration are in agreement with unfolding data reported for acrylodan interaction with HSA, thus leading us to assume that TSPP can bind to domain I of the protein and report alterations therein, Scheme 1. Hemin (iron (II) protoporphyrin IX) was reported to primarily locate in domain I, whereas domains II and III were secondary locations [51]. The analysis of the crystal structure of HSA complexed with hemin and fatty acid provided evidence for hemin location in subdomain IB: the macrocycle bound within a narrow hydrophobic cavity with the propionate groups coordinated by a triad of basic residues at this pocket entrance and the central metal atom coordinated by Tyr^{161} [52]. TSPP does not have a metal atom coordinated and the substitution of four sulfonatophenyl in *meso*-positions contrasts with the two propionate groups in β-positions, in hemin's case, contributing to differences in the amphiphilic nature of both porphyrins. Nonetheless the data presented suggest a number of high affinity hydrophobic sites available for TSPP binding in the folded conformation of HSA and confirm the sequential unfolding of the three domains.

4.2. HSA unfolding process affects TSPP aggregation

The structural changes produced in HSA upon addition of low amounts of Gdn-HCl (<2 M) affects the balance between

monomer ↔ aggregates of TSPP as indicated by changes in the visible extinction and induced CD spectra, at both pH studied. Based on exciton theory one can distinguish between J- (red-shift) and H-aggregates (blue shift) [53]. At pH = 7, the Soret band shifts to the blue and broadens whereas at pH = 2.5 the red-shifted and narrow band at 490 nm increases together with a decrease of the 422 nm band of the bound monomer. These spectral features are consistent with different types of molecular arrangements in the aggregates: a face-to-face packing predominates at pH = 7, whereas a head-to-tail alignment is detected at pH = 2.5 (Scheme 1). While the former was never detected for TSPP in the presence of native HSA at any proportions of the two components nor at any pH studied, J-aggregates can be induced by HSA presence at low HSA/TSPP ratios and low pH. Under these pH conditions, the lateral anionic sulfonatophenyl groups are nearly co-planar with respect to the porphyrin macrocycle which has the two inner nitrogens protonated thus facilitating the interaction between adjacent units and leading to in-line homoassociated arrays [54,55]. The excess of positive charges of HSA at pH = 2.5 minimizes the repulsions between the anionic lateral groups in the porphyrin favouring this J-arrangement [13]. Recently, it was shown that the aggregation properties of the cationic metalloporphyrin, Cu(II) 5,15-bis(N-methylpyridinium-4-yl)-10,15-bis(diphenylporphine) were sensitive to the conformation of the model protein, poly-L-glutamate. Upon pH changes, the α-helix to random coil transition of the polypeptide led to alterations in the porphyrin aggregation which changes from dimers to large J-aggregates [56].

The face-to-face packing in the H-aggregate is not at all favoured at any of the pH conditions used in this work, due to repulsions between the positively charged centers or between the negative peripheral groups. However, this association could be facilitated at pH = 7 in view of the absence of charges in the porphyrin macrocycle together with a nearly orthogonal position of the sulfonate groups. Nonetheless, the aggregation process is triggered only upon addition of Gdn-HCl (up to ~2 M). The existence of nearby accessible residues with positively charged side-chains like lysines or histidines may contribute to the stabilization of such type of aggregate, similar to the interaction of TSPP and polylysine [57]. The overall data supports the idea that the initial unfolding of HSA occurs with separation of domains I and II making positive charges around TSPP more accessible and thus stabilizing porphyrin H-aggregates. These are most probably only dimers since no resonance light scattering (RLS) signal was detected [58].

It is worth mentioning that the porphyrin itself is sensitive to the denaturant presence and ionic nature, but without HSA, only spectral shifts in TSPP absorbance and fluorescence were detected, which are well described by classical dielectric models.

No induced CD was observed in the absence of the protein, ruling out porphyrin aggregation under the conditions used. Therefore, TSPP aggregation depends on the protein conformation and charge balance as confirmed by the induced supramolecular chirality of TSPP at both pHs tested, and proposed in Scheme 1 (see also Fig. S4). A similar Cotton effect had been reported for TSPP interaction with optically active polylysine at pH = 3.1, where the band around 420 nm always followed the polypeptide chirality [59]. One is tempted to justify the opposite signs obtained for the induced CD at pH = 7 and pH = 2.5 with differences in the local chirality of the protein where TSPP aggregation takes place. We cannot disregard the fact that this difference may arise from the distinct orientations of the units in the aggregate supramolecular packing. Substantial changes in TSPP absorbance and fluorescence start at concentrations just above 2 M Gdn-HCl. The decrease in J-aggregate absorbance together with the increase in the monomer Soret band at 443 nm is consistent with a destabilization in porphyrin–porphyrin interactions. The interplay between the stabilizing effect of the positively charged surface of HSA in minimizing the contact between the negatively charged peripheral groups of TSPP and maintaining the porphyrinic arrangement is affected by the excess of Cl^- from the denaturant, at this stage. This agrees with the reported effect of NaCl addition on TSPP aggregation at acidic pH [32]. At Gdn-HCl concentrations above 3 M and regardless the solution pH, HSA adopts an unfolded structure and TSPP is released to the aqueous solution (Scheme 1), as proved by the FCS data. The ensemble of results gives convincing evidence that in the presence of high denaturant concentration the protein does not interact with the porphyrin.

5. Conclusions

The work reported showed that the ligand (TSPP) can exert an important role in inducing conformational changes that contribute to HSA stability namely towards the denaturation by the ionic chaotropic agent Gdn-HCl as well as by the medium acidity. The stabilization was denoted by higher concentrations of Gdn-HCl needed to unfold HSA being maximal at a 1:1 protein/porphyrin ratio. This parallels the increase in α-helix content observed in far-UV CD data and the lesser accessibility of acrylamide to Trp^{214}.

Interestingly, the conformational structure of the intermediate states of HSA affects the equilibrium monomer ↔ aggregate of TSPP. The overall data highlights the possibility of using TSPP as a reporter of conformational changes of HSA only by dealing with noncovalent interactions. These changes could be triggered by varying the pH (forming J-aggregates); by altering inter-domain distances upon denaturant addition (depending on pH TSPP forms J- or H-aggregates); by complete unfolding (no interaction). A higher specificity can even be achieved for the Trp^{214} by following its energy transfer efficiency to TSPP.

Acknowledgements

Professor J. Costa Pessoa is acknowledged for the use of CD spectrometer. S.M.B. Costa and S.M. Andrade acknowledge the financial support from CQE/FCT, projects POCI/QUI/57387/2004, PTDC/QUI/64112/2006, 3° Quadro Comunitário de Apoio (FEDER) and FCT/Re-equipment project 115/QUI/2004.

Appendix A. Supplementary data

Supplementary data associated with this article can be found, in the online version, at doi:10.1016/j.jphotochem.2010.09.028.

References

[1] E.W. Yu, D.E. Koshland Jr., Propagating conformational changes over long (and short) distances in proteins, Proc. Natl. Acad. Sci. U.S.A. 98 (2001) 9517–9520.
[2] P. Ascenzi, M. Fasano, Allostery in a monomeric protein: the case of human serum albumin, Biophys. Chem. 148 (2010) 16–22.
[3] R.F. Pasternack, E.J. Gibbs, S. Sibley, L. Woodard, P. Hutchinson, J. Genereux, K. Kristian, Formation kinetics of insulin-based amyloid gels and the effect of added metalloporphyrins, Biophys. J. 90 (2006) 1033–1042.
[4] T.J. Dougherty, C.J. Gomer, B.W. Henderson, G. Jori, D. Kessel, M. Korbelik, J. Moan, Q. Peng, Photodynamic therapy, J. Natl. Cancer Inst. 90 (1998) 889–905.
[5] X.A. Zhang, K.S. Lovejoy, A. Jasanoff, S.J. Lippard, Water-soluble porphyrins imaging platform for MM zinc sensing, PNAS 104 (2007) 10780–10785.
[6] M. Sibrian-Vazquez, I.V. Nesterova, T.J. Jensen, M.G.H. Vicente, Mitochondria targeting by guanidine- and biguanidine-porphyrin photosensitizers, Bioconjug. Chem. 19 (2008) 705–713.
[7] O. Ohno, Y. Kaizu, H. Kobayashi, J-aggregate formation of a water-soluble porphyrin in acidic aqueous media, J. Chem. Phys. 99 (1993) 4128–4139.
[8] D.L. Akins, H.-R. Zhu, C. Guo, Aggregation of tetraaryl-substituted porphyrins in homogeneous solution, J. Phys. Chem. 100 (1996) 5420–5425.
[9] N.C. Maiti, S. Mazumdar, N. Periasamy, J- and H-aggregates of porphyrin-surfactant complexes: time-resolved fluorescence and other spectroscopic studies, J. Phys. Chem. B 102 (1998) 1528–1538.
[10] S.M. Andrade, S.M.B. Costa, Spectroscopic studies of water-soluble porphyrins with protein encapsulated in bis(2-ethylhexyl) sulfosuccinate (AOT) reverse micelles: aggregation versus complexation, Chem. Eur. J. 12 (2006) 1046–1057.

[11] S.M. Andrade, R. Teixeira, S.M.B. Costa, A.J.F.N. Sobral, Self-aggregation of free base porphyrins in aqueous solution and in DMPC vesicles, Biophys. Chem. 133 (2008) 1–10.
[12] I.E. Borissevitch, T.T. Tominaga, H. Imasato, M. Tabak, Fluorescence and optical absorption study of interaction of two water soluble porphyrins with bovine serum albumin. The role of albumin and porphyrin aggregation, J. Lumin. 69 (1996) 65–76.
[13] S.M. Andrade, S.M.B. Costa, Spectroscopic studies on the interaction of a water soluble porphyrin and two drug carrier proteins, Biophys. J. 82 (2002) 1607–1619.
[14] E. Herczenik, M.F.B.G. Gebbink, Molecular and cellular aspects of protein misfolding and disease, FASEB J. 22 (2008) 2115–2133.
[15] J. Juarez, P. Taboada, V. Mosquera, Existence of different structural intermediates on the fibrillation pathway of human serum albumin, Biophys. J. 96 (2009) 2353–2370.
[16] S. Muzammil, Y. Kumar, S. Tayyab, Anion-induced stabilization of human serum albumin prevents the formation of intermediate during urea denaturation, Proteins 40 (2000) 29–38.
[17] S.S. Krishnakumar, D. Panda, Spatial relationship between the prodan site, trp-214, cys-34 residues in human serum albumin and loss of structure through incremental unfolding, Biochemistry 41 (2002) 7443–7452.
[18] K Flora, J.D. Brennan, G.A. Baker, M.A. Doody, F.V. Bright, Unfolding of acrylodan-labeled human serum albumin probed by steady-state and time-resolved fluorescence methods, Biophys. J. 75 (1998) 1084–1096.
[19] C. Leggio, L. Galantini, P.V. Konarev, N.V. Pavel, Urea-induced denaturation process on defatted human serum albumin and in the presence of palmitic acid, J. Phys. Chem. B 113 (2009) 12590–12602.
[20] D.M. Togashi, A.G. Ryder, D. O'Shaughnessy, Monitoring local unfolding of bovine serum albumin during denaturation using steady-state and time-resolved fluorescence spectroscopy, J. Fluoresc. 20 (2010) 441–452.
[21] X.M. He, D.C. Carter, Atomic structure and chemistry of human serum albumin, Nature 358 (1992) 209–215.
[22] W. Qiu, L. Zhang, O. Okobiah, Y. Yang, L. Wang, D. Zhong, A.H. Zewail, Ultrafast solvation dynamics of human serum albumin: correlations with conformational transitions and site-selected recognition, J. Phys. Chem. B 110 (2006) 10540–10549.
[23] B.P. Esposito, A. Faljoni-Alário, J.F.S. Meneses, H.F. Brito, R. Najjar, A circular dichroism and fluorescence quenching study of the interactions between rhodium(II) complexes and human serum albumin, J. Inorg. Biochem. 75 (1999) 55–61.
[24] C.Z. Huang, Y.F. Li, K.A. Li, S.Y. Tong, Spectral characteristics of the aggregation of α, β, γ, δ-tetrakis(p-sulfophenyl)porphyrin in the presence of proteins, Bull. Chem. Soc. Jpn. 71 (1998) 1791–1797.
[25] S.M. Andrade, S.M.B. Costa, The location of tryptophan, N-acetyltryptophan and α-chymotrypsin in reverse micelles of AOT: a fluorescence study, Photochem. Photobiol. 72 (2000) 444–450.
[26] P. Kapusta, M. Patting, S. Ruttinger, Fluorescence lifetime correlation spectroscopy using the symphotime software: FLCS tutorial, 2008, PicoQuant Application Note, pp. 1–8.
[27] S.T. Hess, W.W. Webb, Focal volume optics and experimental artifacts in confocal fluorescence correlation spectroscopy, Biophys. J. 83 (2002) 2300–2317.
[28] K. Chattopadhyay, S. Saffarian, E.L. Elson, C. Frieden, Measuring unfolding of proteins in the presence of denaturant using fluorescence correlation spectroscopy, Biophys. J. 88 (2005) 1413–1422.
[29] C.N. Pace, Determination and analysis of urea and guanidine hydrochloride denaturation curves, Methods Enzymol. 131 (1986) 266–280.
[30] M.M. Santoro, D.W. Bolen, Unfolding free energy changes determined by the linear extrapolation method. Denaturants, Biochemistry 27 (1988) 8063–8068.
[31] D.R. Lide, Appendix A—Mathematical tables, in: D.R. Lide (Editor-in-Chief), Handbook of Chemistry and Physics, 72nd edition, 1991, CRC Press, Inc.
[32] S.M. Andrade, S.M.B. Costa, Aggregation kinetics of meso-tetrakis(4-sulfonatophenyl) porphine in the presence of proteins: temperature and ionic strength effects, J. Fluoresc. 12 (2002) 77–82.
[33] The type of energy transfer can be derived from the value of R_0, the critical distance at which energy transfer to the acceptor and spontaneous decay of the excited donor are equally probable.
[34] A. Fersht, Structure and Mechanism in Protein Science: A Guide to Enzyme Catalysis and Protein Folding, W.H. Freeman & Co., USA, 1999, Chapter 17, pp. 508–539. *Note*: *m* is proportional to the number of groups in a protein, large proteins are more sensitive to solvent denaturation than small ones, due to bigger changes in surface area on denaturation in the case of the former.
[35] S. Muzammil, Y. Kumar, S. Tayyab, Molten globule-like state of human serum albumin at low pH, Eur. J. Biochem. 266 (1999) 20–32.
[36] Y.H. Chen, J.T. Yang, K.H. Chau, Determination of helix and beta-form of proteins in aqueous solution by circular dichroism, Biochemistry 13 (1974) 3350–3359.
[37] S.M. Andrade, S.M.B. Costa, J.W. Borst, A. Van Hoek, A.J.W.G. Visser, Translational and rotational motions of albumin sensed by a non-covalent associated porphyrin under physiological and acidic conditions: a fluorescence correlation spectroscopy and time resolved anisotropy study, J. Fluoresc. 18 (2008) 601–610.
[38] I. Renge, Solvent dependence of the visible absorption maxima of meso-tetraphenylporphine, Chem. Phys. Lett. 185 (1991) 231–236.
[39] K.A. Schug, W. Lindner, Noncovalent binding between guanidinium and anionic groups: focus on biological- and synthetic-based arginine/guanidinium interactions with phosph[on]ate and sulf[on]ate residues, Chem. Rev. 105 (2005) 67–113.
[40] N. Micali, F. Mallamace, A. Romeo, R. Purrello, L.M. Scolaro, Mesoscopic structure of meso-tetrakis(4-sulfonatophenyl)porphine J-aggregates, J. Phys. Chem. B 104 (2000) 5897–5904.
[41] A. Miura, Y. Shibata, H. Chosrowjan, N. Mataga, N. Tamai, Femtosecond fluorescence spectroscopy and near-field spectroscopy of water-soluble tetra(4-sulfonatophenyl)porphyrin and its J-aggregate, J. Photochem. Photobiol. A: Chem. 178 (2006) 192–200.
[42] P. Schwille, U. Haupts, S. Maiti, W.W. Webb, Molecular dynamics in living cells observed by fluorescence correlation spectroscopy with one- and two-photon excitation, Biophys. J. 77 (1999) 2251–2265.
[43] W. Al-Soufi, B. Reija, S. Felekyen, C.A.M. Seidel, M. Novo, Dynamics of supramolecular association monitored by fluorescence correlation spectroscopy, ChemPhysChem 9 (2008) 1819–1827.
[44] N. El Kadi, N. Taulier, J.Y. Le Huerou, M. Gindre, W. Urbach, I. Nwigwe, P.C. Kahn, M. Waks, Unfolding and refolding of bovine serum albumin at acid pH: ultrasound and structural studies, Biophys. J. 91 (2006) 3397–3404.
[45] M.S. Celej, S.A. Dassie, E. Freire, M.L. Bianconi, G.D. Fidelio, Ligand-induced thermostability in proteins: thermodynamic analysis of ANS–albumin interaction, Biochim. Biophys. Acta 1750 (2005) 122–133.
[46] H.N. Hou, Z.D. Qi, Y.W. OuYang, F.L. Liao, Y. Zhang, Y. Liu, Studies on interaction between vitamin B12 and human serum albumin, J. Pharm. Biomed. Anal. 47 (2008) 134–139.
[47] W. An, Y. Jiao, C. Dong, C. Yang, Y. Inoue, S. Shuang, Spectroscopic and molecular modeling of the binding of meso-tetrakis(4-hydroxyphenyl)porphyrin to human serum albumin, Dyes Pigments 81 (2009) 1–9.
[48] S. Patel, A. Datta, Steady-state and time-resolved fluorescence investigation of the specific binding of two chlorine derivatives with human serum albumin, J. Phys. Chem. B 111 (2007) 10557–10562.
[49] J.K.A. Kamal, L. Zhao, A.H. Zewail, Ultrafast hydration dynamics in protein unfolding: human serum albumin, Proc. Natl. Acad. Sci. U.S.A. 101 (2004) 13411–13416.
[50] B. Ahmad, M.Z. Ahmed, S.K. Haq, R.H. Khan, Guanidine hydrochloride denaturation of human serum albumin originates by local unfolding of some stable loops in domain III, Biochim. Biophys. Acta 1750 (2005) 93–102.
[51] M. Dockal, D.C. Carter, F. Rücker, The three recombinant domains of human serum albumin, J. Biol. Chem. 274 (1999) 29303–29310.
[52] P.A. Zunszain, J. Ghuman, T. Komatsu, E. Tsuchida, S. Curry, Crystal structural analysis of human serum albumin complexed with hemin and fatty acid, BMC Struct. Biol. 3 (2003), http://www.biomedcentral.com/1472-6807/3/6.
[53] E.G. McRae, M. Kasha, Enhancement of phosphorescence ability upon aggregation of dye molecules, J. Chem. Phys. 28 (1958) 271–277.
[54] R. Rubires, J. Crusats, Z. El-Hachemi, T. Jaramillo, M. López, E. Valls, J.-A. Farrera, J.M. Ribó, Self-assembly in water of the sodium salts of meso-sulfonatophenyl substituted porphyrins, New J. Chem. 23 (1999) 189–198.
[55] A.D. Schwab, D.E. Smith, C.S. Rich, E.R. Young, W.F. Smith, J.C. de Paula, Porphyrin nanorods, J. Phys. Chem. B 107 (2005) 11339–11345.
[56] G. De Luca, A. Romeo, L.M. Scolaro, R.F. Pasternack, Conformations of a model protein revealed by an aggregating CuII porphyrin: sensing the difference, Chem. Commun. 46 (2010) 389–391.
[57] R. Purrello, S. Gurrieri, R. Lauceri, Porphryin assemblies as chemical sensors, Coord. Chem. Rev. 190–192 (1999) 683–706.
[58] R.F. Pasternack, C. Bustamante, P.J. Collings, Resonance light-scattering—a new technique for studying chromophore aggregation, Science 269 (1995) 935–939.
[59] L. Zhang, M.H. Liu, Supramolecular chirality and chiral inversion of tetraphenylsulfonato porphyrin assemblies on optically active polylysine, J. Phys. Chem. B 113 (2009) 14015–14020.